RESEARCH ARTICLE

AICHE JOURNAL

Transport Phenomena and Fluid Mechanics

Propulsion efficiency of achiral microswimmers in viscoelastic polymer fluids

David Quashie Jr^{1,2} | David Gordon^{1,2} | Paige Nielsen^{1,2} | Shannon Kelley^{1,2} | Sophie Jermyn^{1,2} | Jamel Ali^{1,2} ⁽¹⁾

Correspondence

Jamel Ali, Department of Chemical and Biomedical Engineering, FAMU-FSU College of Engineering, Tallahassee, FL 32310, USA. Email: jali@eng.famu.fsu.edu

Funding information

Air Force Office of Scientific Research, Grant/Award Number: FA9550-22-1-0247; Grainger Foundation Frontiers of Engineering -NSF, Grant/Award Number: 2000013181; National Science Foundation, Grant/Award Numbers: CMMI-2000330, HDR-2000202; NSF FAMU CREST Center, Grant/Award

Number: HDR-1735968

Abstract

We report the effects of polymer size, concentration, and polymer fluid viscoelasticity on the propulsion kinematics of achiral microswimmers. Magnetically driven swimmer's step-out frequency, orientation angle, and propulsion efficiency are shown to be dependent on fluid microstructure, viscosity, and viscoelasticity. Additionally, by exploring the swimming dynamics of two geometrically distinct achiral structures, we observe differences in propulsion efficiencies of swimmers. Results indicate that larger four-bead swimmers are more efficiently propelled in fluids with significant elasticity in contrast to smaller 3-bead swimmers, which are able to use shear thinning behavior for efficient propulsion. Insights gained from these investigations will assist the development of future microswimmer designs and control strategies targeting applications in complex fluids.

KE YWOR DS

colloids, complex fluids, fluid mechanics, microfluidics, rheology

1 | INTRODUCTION

In the early fifties, Taylor elucidated the coupling between a submerged object and resistive forces in a Stokeslet environment. Since then, swimming locomotion of submerged microscale swimmers in low Reynolds number environments has been the attention of growing experimental and theoretical research. The two primary forms of low Reynolds number swimming explored thus far include (1) rigid chiral filament rotation, inspired by bacterial flagella, and (2) oscillation of flexible filaments, inspired by the eukaryotic cilia and flagella. These investigations have led to artificial actuators that achieve propulsion for biomedical and environmental actuators that achieve propulsion for biomedical and environmental applications. Techniques such as glancing angle deposition have been used to fabricate synthetic actuators; however, one-pot reactions relying on the self-assembly of magnetic colloids can offer a simplistic and scalable manufacturing method.

A myriad of methods have been implemented to realize the propulsion of magnetic microsphere assemblies in low Reynold's environments. One approach uses flexible filaments¹⁸ such as DNA to

link magnetic microspheres, allowing propulsion through time-varying oscillating ¹⁹ and rotating ²⁰ magnetic fields. Less flexible microbead swimmers can also be assembled in the absence of filaments using the particle's magnetic dipole interactions in a static magnetic field. These swimmers of varying bead diameters achieve nonreciprocal motion because of structural deformation within its cyclic motion. ²¹ However, the assembled structure of these flexible swimmers are found to be unstable and achieve low propulsion efficiencies. ²² It has been shown that for non-flexible swimmers, while the shape of an object is essential, the orientation of its transverse magnetic dipole governs swimming. ²³ Recently magnetic microspheres that form rigid assemblies—termed achiral microrobots ²⁴—have been shown to propel themselves when subject to an external magnetic torque.

Rigid swimmers made of clusters of magnetic beads are the simplest achiral propellers and contain at least one plane of symmetry. Achiral swimmers' propulsion and controllability have been demonstrated by Cheang et al., who concluded the minimal requirement for swimming is that the coupling tensor between velocity and torque, G,

¹Department of Chemical and Biomedical Engineering, FAMU-FSU College of Engineering, Tallahassee, Florida, USA

²National High Magnetic Field Laboratory, Tallahassee, Florida, USA

QUASHIE ET AL. stock solutions. The solutions were incubated and shaken at 200RPM overnight to allow humectation of the polymer molecules. A 100 µm filter was then used to remove large debris, followed by a 5 µm poresized filter. The concentrations for the 88 kg/mol MC are chosen to be below the onset of thixotropic behavior, which is expected at 2% w/v.32 The concentrations used for the 15 kg/mol and 44 kg/mol MC polymers were chosen to match the viscosities of the 88 kg/mol concentrations (Figure 1A). In contrast, concentrations for the PAAm and XG were chosen to match their viscosities at 10 s⁻¹. The final concentrations for the polymer fluids used were 15 kg/mol MC: 1, 2, 3% w/v, 44 kg/mol MC: 0.2, 0.6, 0.9% w/v, 88 kg/mol MC: 0.2, 0.4, 0.6% w/v, PAAm: 0.25, 0.5, 0.75% w/v, and XG: 0.075, 0.5, 0.75% w/v, respectively. 1.1.2 Fluid characterization

is nonzero.²⁴ The velocity of these rigid swimmers have also been shown to depend on a geometry-dependent matrix called the chirality matrix, Ch.²³ In addition, Benhal et al. demonstrated that the viscosity of the fluidic environment can also affect the kinematics of 3 and 4 bead chained achiral microswimmers.²⁵ Specifically, in Newtonian fluids, bulk viscosity reduces the propulsion speed and the frequency range at which nonsymmetrical swimming is achieved, while polymer size controls the degree to which propulsion is inhibited.

While magnetic beads' geometry and net magnetization vector have significant control over their propulsion in uniform rotating magnetic fields, viscoelastic properties of the fluidic environment can also dictate the swimming dynamics of rigid microactuators. 26 Through analytical theory and numerical simulations, researchers revealed that while force and torque-free swimmers are unable to propel themselves in a Newtonian fluid, in another fluid possessing viscoelastic properties, the swimmers translate.²⁷ Similarly, a force-free 'snowman' swimmer, comprised of one large and small rotating spheres. experimentally achieved propulsion in Boger fluids via normal stress differences.²⁸ Recent research demonstrates that single magnetic microspheres achieve propulsion due to the rod climbing effect in viscoelastic solutions with first and second normal stress differences.²⁹ The observed motion in polymer fluids with well-defined microstructures results from significant viscoelastic phenomena produced by curved streamlines. 30 These streamlines may generate hoop stresses resulting in nonlinear properties such as local secondary flows in the vicinity of a rotating particle, allowing propulsion enhancement or attenuation

Here we experimentally explore the effect of the fluid microstructure on the dynamics of achiral swimmers by creating polymer solutions with constant bulk viscosity and varying molecular weight. In addition, the effects of viscoelasticity and viscosity are distinguished,31 providing new insight into their impact on achiral microswimmers. Achiral swimmers made of 3 or 4 magnetic microspheres are first fabricated and actuated in Newtonian methylcellulose (MC) solutions. The MC's molecular weight and polymer concentration are varied, illustrating its effects on achiral dynamics. Finally, the achiral swimmers kinematics are further investigated using elastic (polyacrylamide) and shear-thinning (xanthan gum) dominant fluids to determine viscoelastic effects.

1.1 Experimental procedure

Fabrication of polymer fluids 1.1.1

Stock polymer solutions were made using different molecular weights of MC, 3% g/ml (M7140, Millipore Sigma Mn: 15,000 g/mol), 1% g/ml (M0262 Millipore Sigma Mn: 44,000 g/mol), and 1% g/ml (M0512 Millipore Sigma Mn: 88,000 g/mol). Additionally, stock solutions of 2% mg/ml polyacrylamide, PAAm (92,560 Millipore Sigma, Mn: 5-6 x 10⁶ g/mol) and 2% mg/ml xanthan gum, XG (G1253 Millipore Sigma, Mn: 2 x 10⁶ g/mol) were created. DI water purified using PURELAB flex 1 (ELGA LabWater), was used as the solvent for the

Viscosity characterizes the relationship between an applied shear and the fluid's ability to flow. In dilute polymer fluids, viscosity is a function of solvent viscosity, polymer molecular weight and the polymer structure.³³ For all solutions, a rheometer (MCR 302, Anton Paar) with a cone and plate geometry (diameter: 50 mm, angle: 1°) was used to characterize the fluids between shear rates of 0-100 s⁻¹. MC polymer solutions displayed Newtonian behavior having a constant viscosity. The radius of gyration (Rg) and overlap concentration (c*) of the 15 kg/mol, 44 kg/mol, and 88 kg/mol MC polymers were estimated to be ~8.9, 17.5, 26.5 nm and ~9, 3, 1% w/v.34

The PAAm and XG fluids exhibited non-Newtonian behavior (Figure 1C,D) and were fitted to the power-law model $\eta \frac{1}{4} K \gamma_{-}^{n}$. Here η , K, γ_{-} , and n represent the viscosity, flow consistency, shear rate, and Power law constant, respectively. The PAAm's power law constant ranged between 0.92 and 0.98, while the XG's ranged between 0.52 and 0.70. For the Mn of PAAm and XG used, the R_a and c* were estimated to be ~96, 255 nm and ~1.3, 0.94% w/v. 35-38 Thus, the characteristic length scales that define the polymer structure in these fluids are one order of magnitude, or more, smaller than the characteristic length of the swimmers (Figure 2A).

To quantify the elasticity of dilute PAAm and XG polymer solutions multiple particle tracking was used. Video microscopy was accomplished using a Nikon Eclipse Ti2-E equipped with a Plan Fluor 20x objective, Prime 95B 25MM CMOS camera and Lumencor SPEC-TRA X for image sequence acquisition and sample illumination. The optical equipment allowed the recording the thermal fluctuations of 0.5 µm fluorescent tracer particles sealed using a glass slide (25 x 75 x 1.0 mm), coverslip (22 x 22 mm; thickness No. 1) separated by a 120 µm deep spacer. The camera's sensor area was cropped to 1605 by 150 pixels to achieve a sampling frequency of ~600 Hz and exposure time, $\sigma \sim 1$ ms. Image sequences were imported into ImageJ to track the trajectory of in plane particles using the TrackMate plugin. The time evolution of the apparent mean squared displacement (MSD), $(\overline{r^2} \delta \Delta t P) \frac{1}{4} (\frac{1}{8} x \delta t | \Delta t P - x \delta t P)^2 | b \frac{1}{8} y \delta t | \Delta t P - y \delta t P)^2)$, was extracted using the MSD diff classifier function, 39 where x and y represent the

probe's spatial coordinates in two dimensions.

FIGURE 1 Shear rheology. (A) All MC solutions show Newtonian characteristics between 0 and 100 s⁻¹. Low ~3 mPa s, Medium ~10 mPa s, High ~25 mPa s (B) Mean squared displacement (MSD), $\langle r2(\Delta t) \rangle$, obtained from multiple particle tracking for both viscoelastic xanthan gum and polyacrylamide fluids. Viscosity graphed as a function of shear rate for viscoelastic fluids. (C) Xanthan gum, (D) polyacrylamide. All measurements are repeated in triplicate with standard deviation ≤0.3 mPa s.

FIGURE 2 Achiral

microswimmer schematic.

(A) Representation of 3 and 4 bead chained microswimmer translating through different molecular weight polymer solutions with different Rg. Not to scale. (B) Front view of achiral microswimmer showing the

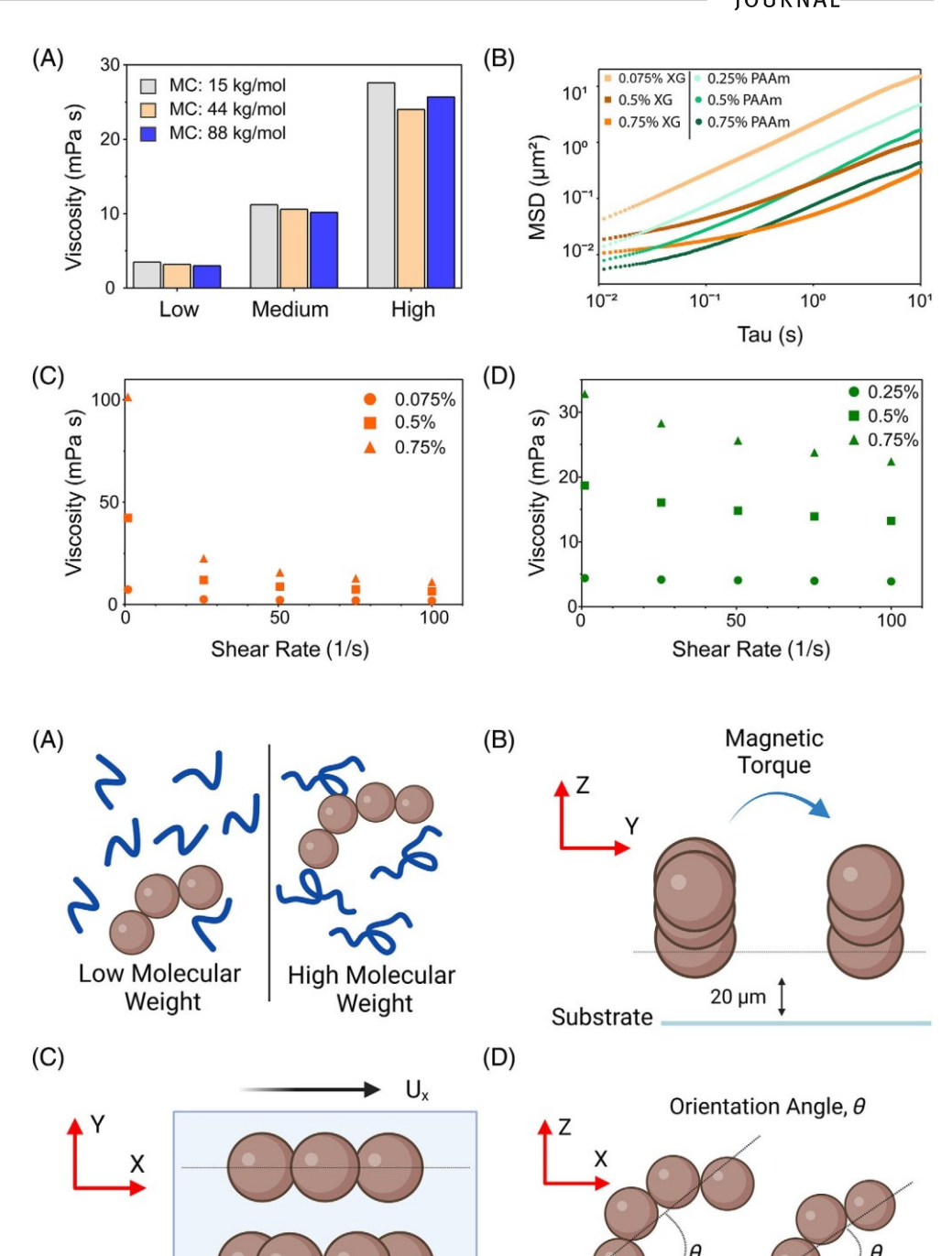
direction of the magnetic field

of the achiral microswimmer

microswimmer being propelled in the x-direction (Ux) (D) Side view

showing the orientation angle (θ). Created using Biorender.

(C) Top view of achiral



To correct for the static error, ε , which is known to give the appearance of viscoelastic effects by creating a plateau at low lag times, probes were fixed to a glass slide to record image sequences of their locations. For our experimental setup the static error was found to be ~51 nm (Figure 1B). In comparison to the static error, correction for dynamic error is nontrivial for non-Newtonian fluids. ⁴⁰ Common considerations for reducing the dynamic error can be achieved by using a low exposure time, ^{41,42} neglect short lag time data, ⁴³ or introducing a correction term for the apparent MSD. ^{40,44} Here we use a combination of the first two methods to reduce dynamic error where

 Δt_{min} is defined as $\Delta t_{min} > 10\sigma$.⁴² The maximum lag time, Δt_{max} is defined where the number of MSD data points becomes less than 10^4 due to lack of statistics at long lag times.⁴³

Quantification of the viscoelasticity of the polymers was achieved using the generalized Stokes-Einstein equation to estimate the fluid's viscoelastic spectrum G $\delta s p$ as a function of the Laplace frequency $s.^{45}$. The viscoelastic spectrum was fitted with $G^{\sim} g p / 4 \frac{G s}{spbrp^{-1}}$ to find the relaxation time coefficient τ and elastic modulus coefficient G. The modulus for PAAm solutions were observed to have a higher range of magnitudes $(0.74-0.87 \, Pa)$ compared to XG $(0.28-0.38 \, Pa)$. The

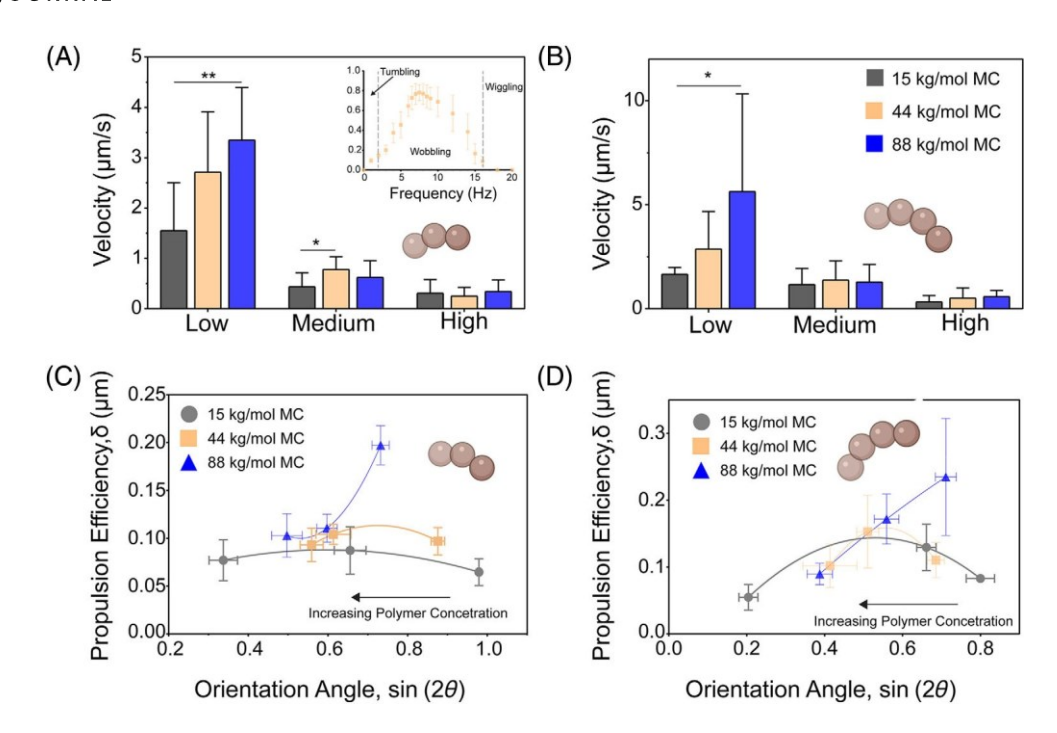


FIG U R E 3 Achiral microswimmer velocity at ω_{s-o} . As the polymer concentration decreases, the propulsion velocity decreases. This trend is seen for all MC fluids. Low ~3 mPa s, Medium ~10 mPa s, High ~25 mPa s (A) 3 bead (B) 4 bead. The inset of (A) identifies the swimming kinematics of the achiral swimmers in 44 kg/mol MC (~10 mPa s). Efficiency vs. $\sin(2\theta c)$ of achiral microswimmers in methylcellulose of varying molecular weight. Data points from left to right indicate increasing the polymer concentration. Here the step-out frequency, ω_{s-o} , is used to normalize its corresponding velocity. (C) 3 bead (D) 4 bead. n = 10 for all data points. $*p \le 0.05$. $**p \le 0.01$.

relaxation times in increasing order of concentration for PAAm solutions were 10.1, 33.1, 76.1 ms, and for XG were 0.4, 124.3, 445.4 ms, respectively.

1.1.3 | Achiral swimmer fabrication

Achiral swimmers were fabricated using 4.35 μ m diameter polystyrene superparamagnetic particles functionalized with either biotin (TM-40-10, Spherotech Inc.) or streptavidin (VM-40-10, Spherotech Inc.). The particles were formed in polymer solutions made of MC, polyacrylamide (PAAm), and xanthan gum (XG). When a static magnetic field was applied, the particles self-assembled, forming curved rigid assemblies (Figure 2A). The 3 and 4 bead swimmers chosen for the experiments have central arc angles less than 180° and at least one axis of symmetry.

1.1.4 | Experimental acquisition

The mixture of achiral swimmers in polymer solutions was then placed in sealed polydimethylsiloxane chambers to prevent the effect of external air flows. The samples were placed on a Nikon Eclipse Ti2 inverted microscope sample holder mounted on the microscope system and were configured with a magnetic field generator (MagnetibotiX MFG-100/100-i) and 40x objective. Using NIS elements software, videos of the 3 and 4 bead achiral swimmers were

acquired at 30 frames per second in their respective fluids. For 3 and 4 bead swimmers in dilute polymer fluids, the velocity, orientation angle and step-out frequency of the achiral swimmers were all extracted using ImageJ as previously described. The propulsion velocity was calculated by dividing the total distance traveled by the time at a given frequency. The orientation angle was measured by the angle of the swimmer centroid from the axis of rotation for the magnetic field (Figure 2D). Finally, a plot of velocity-frequency, was used to identify the step-out frequency, defined as the frequency at which the maximum velocity occurs (Figure 3A inset).

1.2 | Achiral swimmers in polymer fluids

An 8-coil magnetic field generator⁴⁶ was used to apply a uniform rotational magnetic field on the microactuators. Under an external magnetic torque, achiral microswimmers can obtain a chiral-like motion. Here we assume the rotational motion of the achiral swimmers reduce the effect of charged interactions between the nonionic and anionic polymers and swimmers.⁴⁷ As a force-free swimmer, driven explicitly by a magnetic torque, L_m , the translational velocity, U, and angular velocity, Ω , can be described as⁴⁸:

$$U/4G - L_m$$
: $\Omega/4F - L_m$ $\delta 1P$

where $L_m \frac{1}{4} m \times H$ and F, m, H, represent rotational viscous mobility tensor, magnetic dipole moment, and magnetic field amplitude,

respectively. The 3 and 4 bead achiral swimmers' velocity, U, and orientation angle, θ are characterized using frequency sweeps from 1 to 50 Hz at 14 mT (Figure 2C,D). When increasing the frequency at a constant field strength, three swimming regimes (Figure 3A inset) are observed as the swimmers minimize the magnetic energy between their magnetic moment and the applied field.

Initially, there is synchronous tumbling (first regime) where the swimmer rotates in the plane of the applied field (negligible propulsion). Here the swimmers' longitudinal magnetization axis, oriented along its easy axis, follows the external field in-plane. At a critical frequency, the external field superimposes onto the traverse magnetization axis, transitioning the swimmer from tumbling to wobbling (second regime) motion.²³ Here, nonsymmetrical swimming is achieved due to the symmetry-breaking cyclic motion, and the achiral swimmers follow a helical trajectory (translational propulsion). As the frequency increases, the hydrodynamic torque can no longer balance the magnetic torque resulting in a wiggling (third regime) motion (no propulsion). The frequency associated with the onset of this torque imbalance is defined as the step-out frequency ω_{s-o} , where achiral swimmers are known to achieve their maximum translational velocity.

When a rotating achiral swimmer is near a confined wall, in this case underling glass substrate, an increased drag caused by boundary effects leads to drifting. 49 The boundary effects are known to affect the kinematics of achiral swimmers by decreasing the critical frequency and increasing the step-out frequency. To avoid boundary effects, the achiral swimmers are actuated 20 µm above the substrate (Figure 2B).

RESULTS

Optical microscopy is used to track the motion of individual 3 and 4 bead achiral microswimmers in dilute polymer fluids (c < c*). 25 Rotational motion of the achiral swimmers is achieved using a uniform rotational magnetic field at a field strength of 14 mT. The frequency of the magnetic field is incrementally increased from 1 to 50 Hz based on previous work. From the achiral microswimmer's trajectory, the velocity is measured as a function of the magnetic field's frequency. A plot of velocity versus frequency, identifies the critical frequency, resulting in the onset of nonsymmetrical motion, and the step-out frequency resulting in the termination of the nonsymmetrical motion. The orientation angle, θ_c , of the swimmers is determined by the angle of the swimmer centroid from the axis of the rotational magnetic field. In addition, the range of the frequencies used to actuate the achiral swimmers in varying fluid viscosities is determined.

The 3 and 4 bead achiral microswimmers display the three propulsion regimes described in all polymer solutions. The achiral swimmer kinematics can be described using the two modes of transition among the three regimes. The first transition involves the shift from tumbling motion (no propulsion) to wobbling motion (translational propulsion). However, the change between these swimming regimes is mainly controlled by the magnetic properties of the swimmer in addition to the swimmer geometry and fluidic environment. Under a static magnetic field, the easy axis is found to be parallel to the base of the semicircle

structure for the achiral swimmers. The transverse component of magnetization orientation, which is characterized by the azimuthal angle in spherical coordinates, affects the transition between the first and second regime. All things equal, the critical frequency required to switch regimes decreases as the fluid viscosity (polymer concentration) is increased regardless of magnetization orientation and geometry.

The next transition occurs between the second and third regime at which the achiral swimmers reach their ω_{s-o} , the point where the magnetic torque can no longer balance the hydrodynamic drag. Before the onset of this transition, the achiral swimmers retain symmetrybreaking propulsion, and the orientation angle decreases while the propulsion velocity, U, increases with increasing frequency. Here, the ω_{s-a} is determined by selecting the frequency corresponding with the maximal velocity, U_{max} , for 10 of the 3 and 4 bead swimmers. The fluid microstructure is observed to influence the maximal velocity, orientation angle, and step-out frequency. Subsequently, achiral swimmer kinematics will be described using the transition between the second and third regimes.

Overall, for the 15, 44, and 88 kg/mol MC solutions we observe a decrease in the 3 and 4 beads swimmers' step-out frequency, ω_{s-o}, when the polymer concentration is increased. For the 3 bead swimmers the maximum ω_{s-o} occurs at the lowest concentration of the 44 kg/mol MC while the minimum ω_{s-o} occurs in the 44, and 88 kg/ mol at their highest concentration. The decrease in ω_{s-o} correlates with a decrease in the propulsion velocity and orientation angle of the achiral microswimmers. Furthermore, the 4 bead swimmers always maintain a higher propulsion velocity than the 3 bead swimmers in the MC polymer fluids.

Inspection of achiral swimming dynamics at low polymer concentrations (Figure 3A), corresponding to an average viscosity of ~3 mPa s, reveals a monotonic increase in U_{max} and decrease in θ_c as a function of increasing polymer molecular weight. However, we notice that the ω_{s-o} does not follow a similar trend to velocity with varying polymer molecular weight. For example, the 4 bead swimmers have increased propulsion in 44 and 88 kg/mol corresponding with a 30% and 20% increase in ω_{s-o} when compared to the 15 kg/mol polymer solution. The 3 bead swimmers have increased propulsion in 44 kg/mol corresponding to a 17% increase in ω_{s-o}. However, 3 bead swimmers ω_{s-o} is observed to decrease by 29% when compared to the ω_{s-o} in the 88 kg/mol to the 15 kg/mol solution. This result is counterintuitive as one would expect higher ω_{s-o} values to correspond to faster propulsion velocities. As the MC polymer concentrations increase to higher viscosities (\sim 10 and 25 mPa-s) both the U_{max} and θ_c become comparable.

To gain further insight into the aforementioned results, we compare both propulsion velocity and orientation angle at ω_{s-o} , in the synchronous region as²³:

$$\frac{1}{a} \frac{U_{max}}{\omega_{s-o}} \frac{1}{\sqrt{4}} \frac{1}{\delta} \frac{1}{\delta} \frac{1}{\sqrt{4}} C^{\sim} h \sin \delta \psi + \sin \delta 2\theta e^{\frac{1}{\delta}}$$

$$\frac{1}{a} \frac{U_{max}}{\omega_{s-o}} \frac{1}{\sqrt{4}} \frac{1}{\delta} \frac{1}{\sqrt{4}} C^{\sim} h \sin \delta \psi + \sin \delta 2\theta e^{\frac{1}{\delta}}$$

in which a, $C^{\sim}h$, and ψ represents the particle size, pseudo chirality coefficient, and Euler angle, respectively. Normalizing the velocity at

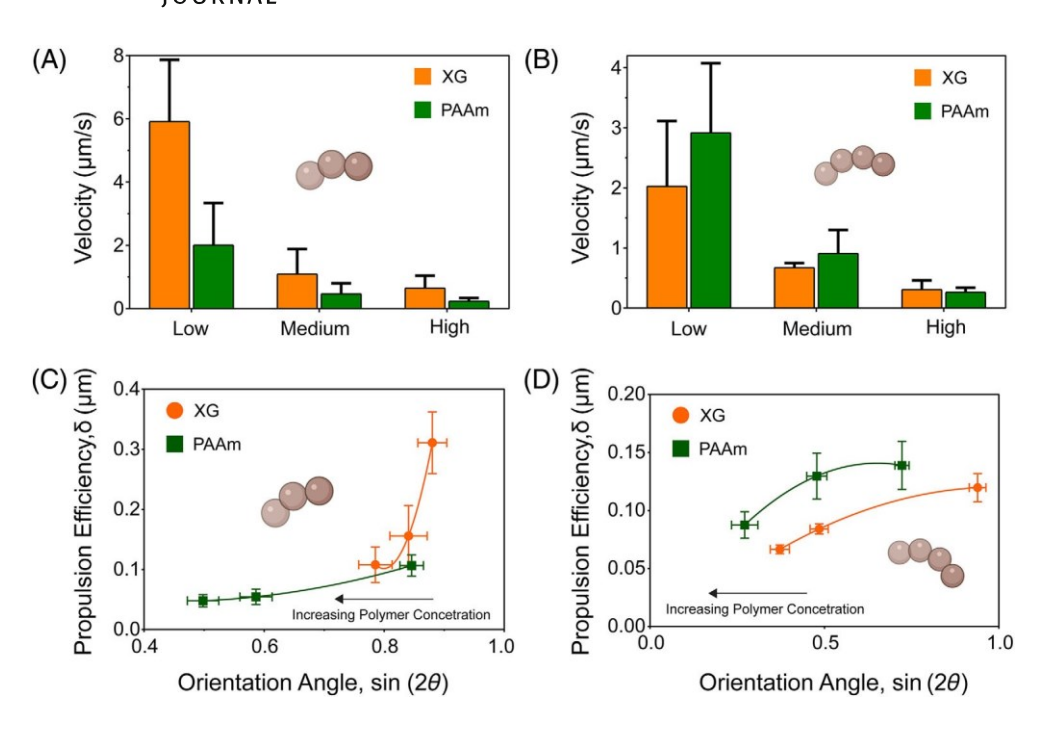


FIGURE 4 Achiral microswimmer velocity at ω_{s-o}. As the viscosity increases, the propulsion velocity decreases. This trend is seen for all fluids. Low ~17 mPa s, Medium ~25 mPas, High ~34 mPas at 10 Hz (A) 3 bead (B) 4 bead. Efficiency vs. sin(2θc) of achiral microswimmers in Polyacrylamide (green) and Xanthan Gum (orange). Here the step-out frequency, ω_{s-o}, is used to normalize its corresponding velocity. (C) 3 bead, (D) 4 bead. n = 5 for all data points.

the step-out frequency gives the propulsion efficiency, δ , of a microswimmer. Achiral swimmers driven by pseudochiral (off-diagonal) terms of the chirality matrix achieve efficient propulsion through orientation of its magnetization axis and geometry of its arc central angle resulting in wobbling. For example, in water, a 3 bead swimmer having an orientation angle of 45° and a central arc angle of 123° would achieve optimal efficiency. We would achieve optimal efficiency.

The relationship between propulsion efficiency and orientation angle for all swimmers (Figure 3C,D) demonstrates the dependence on MC polymer concentration, molecular weight, and swimmer geometry. Interestingly, in the 15 and 44 kg/mol MC solutions, the 3 and 4 bead swimmer's propulsion efficiency remains relatively constant showing minor dependence on polymer concentration within the range of concentrations used. The averaged propulsion efficiency for the 3 and 4 bead swimmers in the 15 kg/mol are $0:076 \pm 0:009 \,\mu m$ and $0.089 \pm 0.031 \,\mu\text{m}$, respectively. When the molecular weight is increased to 44 kg/mol the averaged propulsion efficiency for the 3 and 4 bead swimmers increases to 0:098 \pm 0:005 μm and $0.122 \pm 0.022 \,\mu m$. Swimmers in the 88 kg/mol MC are observed to have swimming profiles that diverge from the 15 and 44 kg/mol MC solutions. A decrease in orientation angle in this fluid is associated with a continuous decrease in propulsion efficiency, which we attribute to local non-Newtonian effects. Hence, the optimal orientation and arc angle requirement can be modified by viscoelastic effects. The two main non Newtonian effects expected for 88 kg/mol MC are elasticity and shear-thinning viscosity. It is difficult to separate the two properties explicitly using MC; thus, we choose elastic dominant (polyacrylamide) and shear-thinning dominant (xanthan gum) fluids to investigate how viscoelasticity affects achiral swimmer propulsion. In the non-Newtonian fluids, frequency sweeps of five 3 and 4 bead swimmers are conducted to determine the kinematics at the step-out frequency.

Similar to the MC solutions, an increase in polymer concentration is observed to decrease both the propulsion velocity (Figure 4A,B) and orientation angles of the swimmers in viscoelastic fluids. For individual viscoelastic fluids, the trend for propulsion velocities is only significant between the low viscosity and medium/ high viscosity solutions $(p \le 0.01)$ with the exception of the 3 bead swimmers in PAAm, which shows no statistical significance ($p \le 0.50$). However, the viscoelastic properties of polyacrylamide (PAAm) and xanthan gum (XG) fluids allow the achiral swimmers to attain large orientation angles. For example, in the low viscosity (17 mPa s) PAAm, the deformation of the polymer due to curved streamlines orients the 3 and 4 bead swimmers to 29° and 23°, respectively. This corresponds to a 26% and 4.5% increase in orientation angle compared to the 88 kg/mol MC solution. Conversely, in XG, the rigidity of the polymer causes the chains to align with the local flow reducing the viscosity.⁵¹ The interaction between swimmer and XG polymers at low viscosities increases the orientation of the 3 and 4 bead swimmers by 34.8% and 59% when related to the 88 kg/mol MC solution.

In the non-Newtonian fluids, the achiral swimmers' highest orientation angles correspond to their highest propulsion efficiency (Figure 4C,D), similar to what is observed in the 88 kg/mol MC polymer fluids. Increasing polymer concentration reduces the magnitude of the orientation angle; however, the 3 bead swimmers in XG at $\omega_{s^{-}o}$ are able to maintain orientation angles greater than 25°. Additionally, the 3 and 4 bead swimmers achieve maximum efficiency in fluids with different viscoelastic effects. The propulsion efficiency in viscoelastic fluids can also be described as a function of the nondimensional Deborah number (De) which describes the ratio of the polymer and swimmer time scales. The polymer fluid's relaxation time, τ , and swimmer's averaged step-out frequency is used to define the De by $De \frac{1}{2}\tau - \omega_{s^{-}o}$. Within the range of De (0.008-1.337) a monotonic decrease in propulsion efficiency is seen for the increase De. However, this decrease

FIG URE 5 Propulsion efficiency of (A) 3 and (B) 4 bead achiral swimmers in dilute polymeric fluids. Propulsion efficiency, which is shown to be dependent on swimmer orientation angle, size, polymer molecular weight, and concentration, is graphed as a function of viscosity. Viscosity here is taken from bulk shear rheology at shear rates corresponding to swimmer step out frequency.

not seen for the 4 bead swimmers in the highest concentration of PAAm (0.75% w/v) whose De and propulsion efficiency both decreases when compared to the 0.5% w/v PAAm solution.

3 | DISCUSSION

To distinguish between viscosity and viscoelasticity, it is instructive to plot the propulsion efficiency as a function of viscosity (Figure 5A,B). For the non-Newtonian fluids, viscosities are selected corresponding to the value at which the achiral swimmers achieve their $\omega_{s-\rho}$. Generally, as the viscosity increases, the propulsion efficiency either remains approximately constant or is hindered based on the orientation angle, as shown earlier (Figures 3C,D and 4C,D). Describing propulsion efficiency as the ratio of energy consumed moving forward versus wobbling provides intuition for the observed trends.⁵² In polymer fluids with low molecular weight (≤44 kg/mol), swimmers' propulsion efficiency is maintained when their orientation angle is constrained. However, maximum efficiency is synonymous with a large orientation angle when the polymer chains are longer. We propose that the achiral swimming enhancement in the high molecular weight MC fluids results from the nonuniform distribution of the MC polymers in the local vicinity of the swimmers. 47,53,54 When the polymer chains are short, the local homogeneity causes a depletion layer allowing the achiral swimmers to achieve significant wobbling, reducing their translational velocity. As the viscosity of the MC fluids is increased (~10 mPas), their ω_{s-o} and θ_c becomes similar and high propulsion velocities are still maintained in the larger molecular weight solutions. However, a greater increase in MC polymer concentration causes the viscous effects to dominate, making their velocities and efficiencies comparable.

To investigate viscoelastic effects specifically, we isolate the propulsion efficiencies at ~3 mPa s. Generally, achiral swimmers that experience non-Newtonian effects attain higher efficiencies. Being able to propel efficiently at high orientation angles can be explained by the elastic response of the fluids. Binagia et al. remarked that for swimmers that generate substantial swirl in elastic polymer fluids, the extensional flow behind the swimmer is disrupted, leading to higher propulsion velocities. ⁵⁵ They also explained that shear thinning

viscosity diminishes the enhancement of swimmers that produce swirling flow. This can be used to describe the achiral 4 bead higher propulsion efficiencies in PAAm versus XG polymer fluids despite having the same ω_{s-o} . The elastic fluid behavior does not explain why 3 bead swimmers have enhanced propulsion in XG polymer fluids. For the 3 bead swimmers, we postulate that shear-thinning viscosity may be responsible for the enhanced efficiency. Unlike flagellated bacteria, whose body and tail rotate at different rates creating high and low viscosity regions enhancing propulsion, 56 our rigid 3 bead swimmer rotates synchronously. Demir et al. proposed that for swimmers that yield a helical trajectory, considerable enhancement can be achieved by nonlocal shear-thinning effects.⁵⁷ For the lowest XG polymer concentration, the 3 bead swimmers maintain the lowest ω_{s-o} , at a value of 19 Hz, causing a viscosity gradient to decay rapidly from the swimmer resulting in an anisotropic drag. This significant local confinement effect leads the achiral swimmers to achieve a higher propulsion efficiency compared to all other swimmer-fluid combinations. Therefore, the 3 bead swimmers prominent propulsion efficiencies in XG, are a result of the nonlocal shear-thinning (confinement) effects.

The 88 kg/mol MC polymer fluids exhibit both elastic and shearthinning viscosity behavior when the achiral swimmers experience a magnetic torque. The 3 bead swimmers decrease in step-out frequency compared with the 15 kg/mol MC fluid at low concentrations demonstrates the shear thinning characteristics of the long-chained methylcellulose polymers. When swimmer size and polymer concentration are increased, there is a competition among elastic, shear thinning, and viscous effects, which can aid or hinder the swimmers propulsive velocity. More dominant viscoelastic effects and additional magnetic material allows the 4 bead swimmers to manifest greater rotational isotropy and achieve higher propulsion efficiencies. Hence, we propose that swimmers in the 88 kg/mol MC fluids propel efficiently with large orientation angles due to local non-Newtonian effects.

4 | CONCLUSION

Here we investigated the propulsion efficiency of 3 and 4 bead achiral microswimmers in polymer fluids and observe that increasing polymer

15475905, 0, Downloaded from https://aiche.onlinelibrary.wiley.com/doi/10.1002/aic.17988 by Florida State University, Wiley Online Library on [17/12/2022]. See the Terms) on Wiley Online Library for rules of use; OA articles are governed by the applicable Creative Commons

molecular weight and concentration can affect the swimming kinematics of these rigid structures, depending on their size and geometry. Swimmer propulsion efficiency and orientation angle are coupled using the geometric dependent pseudochiral equation (Equation 2). In low molecular weight MC (≤44 kg/mol), the orientation angle does not significantly affect the propulsion efficiency, however as polymer molecular weight increases, non-Newtonian effects allow the achiral microswimmers to propel more efficiently at high orientation angles. This behavior was further explored using elastic dominant (PAAm) and shear thinning dominant (XG) polymer fluids. Elasticity mainly contributed to the efficiency enhancement of 4 bead swimmers, while nonlocal shear-thinning fluid behavior enhanced the 3 bead swimmers translation. Hence, these results indicate that swimmers made of popular⁵⁸ 3 and 4 bead achiral geometries can propel efficiently by either increasing viscosity or adding viscoelastic effects. Thus, when designing microswimmers, the swimmer size and non-Newtonian characteristics of the microenvironment need to be considered to achieve maximum propulsion efficiency. To enable the development of optimal achiral microswimmer designs, future work should focus on the dynamics of swimmers in nonlinear fluids with specific central arc angles and determine the role of local polymer depletion layers on propulsion using micro-Particle Imaging Velocimetry (µPIV).

AUTHOR CONTRIBUTIONS

David Quashie Jr: Conceptualization (supporting); data curation (lead); formal analysis (lead); investigation (equal); methodology (lead); validation (equal); visualization (lead); writing - original draft (lead); writing - review and editing (lead). David Gordon: Investigation (supporting); validation (equal); writing - review and editing (equal). Paige Nielsen: Investigation (supporting); validation (equal); writing - review and editing (equal). Shannon Kelley: Investigation (supporting); validation (equal); writing - review and editing (equal). Sophie Jermyn: Investigation (supporting); validation (equal); writing - review and editing (equal). Jamel Ali: Conceptualization (lead); funding acquisition (lead); project administration (lead); resources (lead); supervision (lead); validation (equal); writing - review and editing (equal).

ACKNOWLEDGMENTS

This work was funded by the National Science Foundation (No. HDR-2000202 and CMMI-2000330) and supported by the NSF FAMU CREST Center award (No. HDR-1735968). This research work was also supported by The Grainger Foundation Frontiers of Engineering Grant under the National Academy of Sciences Award Number: 2000013181. This material is based upon work supported by the Air Force Office of Scientific Research under award number FA9550-22-1-0247. All the work was performed at the National High Magnetic Field Laboratory, which is supported by National Science Foundation Cooperative Agreement No. DMR-1644779 and the State of Florida.

The content is solely the responsibility of the authors and does not necessarily represent the official views of The Grainger Foundation or the National Academy of Sciences. Any opinions, findings, and conclusions or recommendations expressed in this material are those of the author(s) and do not necessarily reflect the views of the United States Air Force.

Figure 2 was made with Biorender (biorender.com).

DATA AVAILABILITY STATEMENT

The data that support the findings of this study are available from the corresponding author upon reasonable request.

ORCID

Jamel Ali https://orcid.org/0000-0002-2997-1981

REFERENCES

- Taylor Gl. Analysis of the swimming of microscopic organisms. Proc Royal Soc A: Math Phys Sci. 1951;209(1099):447-461.
- Patteson AE, Gopinath A, Goulian M, Arratia PE. Running and tumbling with E. coli in polymeric solutions. Sci Rep. 2015;5(1):15761.
- Xu H, Medina-Sánchez M, Maitz MF, Werner C, Schmidt OG. Sperm micromotors for cargo delivery through flowing blood. ACS Nano. 2020;14(3):2982-2993.
- Huang HW, Uslu FE, Katsamba P, Lauga E, Sakar MS, Nelson BJ. Adaptive locomotion of artificial microswimmers. Sci Adv. 2019;5(1): eaau1532.
- Cortez R, Fauci L, Medovikov A. The method of regularized stokeslets in three dimensions: analysis, validation, and application to helical swimming. *Phys Fluids*. 2005;17(3):031504.
- Rodenborn B, Chen C-H, Swinney HL, Liu B, Zhang HP. Propulsion of microorganisms by a helical flagellum. *Proc Natl Acad Sci.* 2013; 110(5):E338.
- Solovev A, Friedrich BM. Lagrangian mechanics of active systems. Eur Phys J E. 2021;44(4):49.
- Berg HC, Anderson RA. Bacteria swim by rotating their flagellar filaments. *Nature*. 1973;245(5425):380-382.
- Yasa O, Erkoc P, Alapan Y, Sitti M. Microalga-powered microswimmers toward active cargo delivery. Adv Mater. 2018;30(45):1804130.
- Coq N, Bricard A, Delapierre F-D, et al. Collective beating of artificial microcilia. *Phys Rev Lett*. 2011;107(1):014501.
- Kim S, Qiu F, Kim S, et al. Fabrication and characterization of magnetic microrobots for three-dimensional cell culture and targeted transportation. Adv Mater. 2013;25(41):5863-5868.
- Wei T, Li J, Zheng L, et al. Development of a cell-loading microrobot with simultaneously improved degradability and mechanical strength for performing In vivo delivery tasks. Adv Intell Syst. 2021;3:2100052.
- Singh AK, Bhuyan T, Maity S, Mandal TK, Bandyopadhyay D. Magnetically actuated carbon soot nanoparticle-based catalytic CARBOts coated with Ni/Pt nanofilms for water detoxification and oil-spill recovery. ACS Appl Nano Mater. 2020;3(4):3459-3470.
- Ma W, Wang H. Magnetically driven motile superhydrophobic sponges for efficient oil removal. Appl Mater Today. 2019;15: 263-266.
- Ghosh A, Fischer P. Controlled propulsion of artificial magnetic nanostructured propellers. Nano Lett. 2009;9(6):2243-2245.
- Yamanaka T, Arai F. Self-propelled swimming microrobot using electroosmotic propulsion and biofuel cell. *IEEE Robot Autom Lett.* 2018; 3(3):1787-1792.
- Cheang UK, Ali J, Kim H, Rogowski L, Kim MJ. On-surface locomotion of particle based microrobots using magnetically induced oscillation. *Micromachines*. 2017;8(2):46.
- Yang T, Sprinkle B, Guo Y, et al. Reconfigurable microbots folded from simple colloidal chains. *Proc Natl Acad Sci.* 2020;117(31):18186-18193.

- 19. Dreyfus R, Baudry J, Roper ML, Fermigier M, Stone HA, Bibette J. Microscopic artificial swimmers. Nature. 2005;437(7060):862-865.
- 20. Zaben A, Kitenbergs G, Ce-bers A. 3D motion of flexible ferromagnetic filaments under a rotating magnetic field. Soft Matter. 2020;16(18): 4477-4483.
- 21. Li Y-H, Chen S-C. The dynamics of a planar beating micro-swimmer constructed using functional fluid. J Intell Mater Syst Struct. 2020; 32(12):1358-1367.
- 22. Li YH, Chen SC. Propulsion mechanism of flexible microbead swimmers in the low reynolds number regime. Micromachines. 2020;
- 23. Morozov KI, Mirzae Y, Kenneth O, Leshansky AM. Dynamics of arbitrary shaped propellers driven by a rotating magnetic field. Phys Rev Fluids. 2017;2(4):044202.
- 24. Cheang UK, Meshkati F, Kim D, Kim MJ, Fu HC. Minimal geometric requirements for micropropulsion via magnetic rotation. Phys Rev E. 2014;90(3):033007.
- 25. Benhal P, Quashie D, Cheang UK, Ali J. Propulsion kinematics of achiral microswimmers in viscous fluids. Appl Phys Lett. 2021;118(20):
- Lauga E. Locomotion in complex fluids: integral theorems. Phys Fluids. 2014;26(8):081902.
- 27. Binagia JP, Shagfeh ESG. Self-propulsion of a freely suspended swimmer by a swirling tail in a viscoelastic fluid. Phys Rev Fluids. 2021;6(5):
- 28. Puente-Velázquez JA, Godínez FA, Lauga E, Zenit R. Viscoelastic propulsion of a rotating dumbbell. Microfluid Nanofluid. 2019;23(9):108.
- Rogowski LW, Ali J, Zhang X, Wilking JN, Fu HC, Kim MJ. Symmetry breaking propulsion of magnetic microspheres in nonlinearly viscoelastic fluids. Nat Commun. 2021:12(1):1116.
- 30. Pakdel P, McKinley GH. Elastic instability and curved streamlines. Phys Rev Lett. 1996;77(12):2459-2462.
- 31. Li C, Qin B, Gopinath A, Arratia PE, Thomases B, Guy RD. Flagellar swimming in viscoelastic fluids: role of fluid elastic stress revealed by simulations based on experimental data. J R Soc Interface. 2017; 14(135):20170289.
- 32. Herráez-Domínguez JV, Leo,n FGG, Díez-Sales O, Herráez-Domínguez M. Rheological characterization of two viscosity grades of methylcellulose: an approach to the modeling of the thixotropic behaviour. Colloid Polym Sci. 2005;284(1):86-91.
- 33. Flory PJ. Viscosities of linear polyesters. An exact relationship between viscosity and chain length. J Am Chem Soc. 1940;62(5):
- 34. Striggow F, Medina-Sánchez M, Auernhammer GK, Magdanz V, Friedrich BM, Schmidt OG. Sperm-driven micromotors moving in oviduct fluid and viscoelastic media. Small. 2020;16(24):2000213.
- 35. Zhang H, Feng Y. Dependence of intrinsic viscosity and molecular size on molecular weight of partially hydrolyzed polyacrylamide. J Appl Polym Sci. 2021;138(34):50850.
- 36. Koser AE, Pan L, Keim NC, Arratia PE. Measuring material relaxation and creep recovery in a microfluidic device. Lab Chip. 2013;13(10): 1850-1853.
- 37. Pereira AS, Andrade RM, Soares EJ. Drag reduction induced by flexible and rigid molecules in a turbulent flow into a rotating cylindrical double gap device: comparison between poly (ethylene oxide), polyacrylamide, and xanthan gum. J Non-Newton Fluid Mech. 2013;202:
- Merino-González A, Kozina A. Influence of aggregation on characterization of dilute xanthan solutions. Int J Biol Macromol. 2017;105: 834-842.

- 39. Curtis C, Rokem A, Nance E. Parallelization of multi-particle tracking video analyses. J Open Source Softw. 2019;4(36):989.
- Savin T, Doyle PS. Role of a finite exposure time on measuring an elastic modulus using microrheology. Phys Rev E. 2005;71(4):041106.
- 41. Schultz KM, Furst EM. Microrheology of biomaterial hydrogelators. Soft Matter. 2012;8(23):6198-6205.
- 42. Furst EM, Squires TM. Microrheology. 1st ed. Oxford University Press; 2017.
- 43. Struntz P, Weiss M. The hitchhiker's guide to quantitative diffusion measurements. Phys Chem Chem Phys. 2018;20(45):28910-28919.
- Savin T, Doyle PS. Static and dynamic errors in particle tracking microrheology. Biophys J. 2005;88(1):623-638.
- 45. Mason TG. Estimating the viscoelastic moduli of complex fluids using the generalized Stokes-Einstein equation. Rheol Acta. 2000;39(4):
- 46. Schuerle S, Erni S, Flink M, Kratochvil BE, Nelson BJ. Threedimensional magnetic manipulation of micro- and nanostructures for applications in life sciences. IEEE Trans Magn. 2013;49(1):321-330.
- 47. Qi K. Westphal E. Gompper G. Winkler RG. Enhanced rotational motion of spherical Squirmer in polymer solutions. Phys Rev Lett. 2020:124(6):068001.
- 48. Chen Z, Wang Z, Quashie D, et al. Propulsion of magnetically actuated achiral planar microswimmers in Newtonian and non-Newtonian fluids. Sci Rep. 2021;11(1):21190.
- 49. Wang Q, Yang L, Yu J, Zhang L. Characterizing dynamic behaviors of three-particle paramagnetic microswimmer near a solid surface. Robotics Biomim. 2017;4(1):20.
- 50. Mirzae Y, Dubrovski O, Kenneth O, Morozov Konstantin I, Leshansky AM. Geometric constraints and optimization in externally driven propulsion. Sci Robotics. 2018;3(17):eaas8713.
- 51. Montenegro-Johnson TD, Smith DJ, Loghin D. Physics of rheologically enhanced propulsion: different strokes in generalized Stokes. Phys Fluids. 2013;25(8):081903.
- 52. Lobaskin V, Lobaskin D, Kuli,c IM. Brownian dynamics of a microswimmer. Eur Phys J Spec Top. 2008;157(1):149-156.
- 53. Zöttl A, Yeomans JM. Enhanced bacterial swimming speeds in macromolecular polymer solutions. Nat Phys. 2019;15(6):554-558.
- 54. Fan T-H, Dhont JKG, Tuinier R. Motion of a sphere through a polymer solution. Phys Rev E. 2007;75(1):011803.
- 55. Binagia JP, Phoa A, Housiadas KD, Shaqfeh ESG. Swimming with swirl in a viscoelastic fluid. J Fluid Mech. 2020;900:A4.
- 56. Qu Z, Breuer KS. Effects of shear-thinning viscosity and viscoelastic stresses on flagellated bacteria motility. Phys Rev Fluids. 2020;5(7): 073103.
- 57. Demir E, Lordi N, Ding Y, Pak OS. Nonlocal shear-thinning effects substantially enhance helical propulsion. Phys Rev Fluids. 2020;5(11):
- Song X, Chen Z, Zhang X, et al. Magnetic tri-bead microrobot assisted near-infrared triggered combined photothermal and chemotherapy of cancer cells. Sci Rep. 2021;11(1):7907.

How to cite this article: Quashie D Jr, Gordon D, Nielsen P, Kelley S, Jermyn S, Ali J. Propulsion efficiency of achiral microswimmers in viscoelastic polymer fluids. AIChE J. 2022; e17988. doi:10.1002/aic.17988